The Astronomical Journal, 167:266 (11pp), 2024 June https://doi.org/10.3847/1538-3881/ad3a64

Parallax Effect in Microlensing Events Due to Free-floating Planets

Parisa Sangtarash and Sedighe Sajadian
Department of Physics, Isfahan University of Technology, Isfahan 84156-83111, Iran; s.sajadian@iut.ac.ir
Received 2024 January 27; revised 2024 March 17; accepted 2024 April 2; published 2024 May 15

Abstract

One of the most important applications of microlensing observations is the detection of free-floating planets (FFPs). The timescale of microlensing due to FFPs ($t_{\rm E}$) is short (a few days). Discerning the annual parallax effect in observations of these short-duration events due to FFPs by one observer is barely possible, though their parallax amplitude is larger than that in common events. In microlensing events due to FFPs, the lens–source relative trajectory alters because of the observer's motion by $\boldsymbol{\delta u}$. This deviation is a straight line as long as $t_{\rm E} \ll P_{\oplus}$, and its size is $\delta u \propto \pi_{\rm rel}$ ($P_{\oplus}$ is the observer's orbital period). So, most observed microlensing events due to close FFPs have simple Paczyński light curves with indiscernible but important parallax. To evaluate the destructive effects of invisible parallax in such events, we simulate ∼9650 microlensing events due to FFPs with $t_{\rm E} < 10$ days that are observed only by the Nancy Grace Roman Space Telescope (Roman). We conclude that in half of these microlensing events the missing parallax alters the real light curves, changing their shape and derived properties (by $\Delta\chi^2 \gtrsim 100$). By fitting Paczyński light curves to these affected events we evaluate the relative and dimensionless deviations in the lensing parameters from their real values ($\delta t_{\rm E}$, $\delta\rho_{\star}$, ...). We conclude that around 46 FFPs that are discovered by Roman have light curves highly affected by invisible parallax with $\delta t_{\rm E} > 0.1$ and $\delta\rho_{\star} > 0.1$. Our study reveals the importance of simultaneous and dense observations of the same microlensing events viewed by Roman by other observers circling the Sun in different orbits.

Unified Astronomy Thesaurus concepts: Gravitational microlensing exoplanet detection (2147); Microlensing parallax (2144); Gravitational microlensing (672); Annual microlensing parallax (2149); Free floating planets (549)

1. Introduction

The annual parallax effect is referred to the rotation of the Earth (the observer) around the Sun, which creates additional and apparent motions for stars that are nearby in the plane of the sky. Due to the parallax effect, the angular position of a star at a distance of 1 kpc from us will alter by 2 mas in 6 months as measured from the Earth. Based on these apparent displacements of stars that are nearby in the plane of the sky, some people have even determined their distance from the Earth. Therefore, in astrophysical textbooks, the parallax effect has been introduced as one of the primary methods for measuring the distances of nearby stars (e.g., Carroll & Ostlie 2006). In this way, the Hipparcos and Gaia telescopes have respectively measured the distances of over 100,000 stars and around 1.5 billion stars in the Galaxy based on parallax measurements (Perryman et al. 1997; Gaia Collaboration et al. 2023).

Additionally, the parallax effect alters transient astrophysical events from Galactic stars, because it alters stellar trajectories from straight to cycloid ones (see, e.g., Alcock et al. 1995). The parallax-induced deviations in such events depend on two factors: (a) the distances of the stars from the observer, and (b) the durations of events. The angular extra motions of stars due to the parallax effect are scaled by $\pi_{\star} = 1\ {\rm au}/D$, where D is the stellar distance from the observer. Also, the maximum displacements owing to the parallax effect occur in 6 months. Hence, in short-duration events (e.g., 1–2 days) from distant stars the parallax-induced deviations and bending of stellar trajectories from straight ones are barely recognizable.

One example of transient astrophysical phenomena is gravitational microlensing. This refers to the temporary increase in brightness of a background star in the Galaxy because its light passes through the gravitational potential of a foreground and collinear object (Einstein 1936; Liebes 1964; Refsdal 1964). The most common lenses in gravitational microlensing events toward the Galactic bulge are M dwarfs with masses of $\sim 0.3\,M_{\odot}$. These lens objects create microlensing events that last on average ∼20–30 days (see, e.g., Dominik et al. 2008; Gaudi 2012). In a simple microlensing event the magnification factor depends on three parameters: (i) $\rho_{\star}$, the source radius normalized to the Einstein radius and projected on the plane of the sky, (ii) the brightness profile of the source disk, and (iii) u, the lens–source relative trajectory normalized to the Einstein radius. Here, the Einstein radius is the radius of the image's ring at the time of complete alignment between the lens, the source, and the observer's line of sight. In these events, the parallax effect alters u from a straight line to a cycloid. The amplitude of parallax-induced deviations in the lens–source trajectory is $\pi_{\rm E}$ (the so-called parallax amplitude). Discerning this parallax amplitude helps to resolve the known microlensing degeneracy, since $\pi_{\rm E}$ is a degenerate function of the lens mass and its distance (e.g., Refsdal 1966; Gould 1992; Smith et al. 2005). In joint ground-based and space-based observations of microlensing events, measuring up to three physical parameters of lenses is possible because of different parallax effects seen by different observers (Gould 1994, 1995, 1999). Some examples of realizing satellite parallax in real microlensing observations that one can study are those by An et al. (2002), Shvartzvald et al. (2019), Hirao et al. (2020), and Zang et al. (2020).

One special class of microlensing events are those due to free-floating planets (FFPs), which have short durations (up to a few days; e.g., Sumi et al. 2011; Mróz et al. 2017, 2020;

Koshimoto et al. 2023). In these events, (i) the parallax amplitude is larger than that in common microlensing events due to M dwarfs, and (ii) the observer's trajectory with respect to the Sun is almost a straight line with negligible bending. Therefore, in such events the straight lens–source relative trajectory varies with a considerable and straight deviation, i.e., $\boldsymbol{u}_{\odot} + \boldsymbol{\delta u}$. Accordingly, the parallax effect in these events alters the real light curves to other simple ones with indistinguishable parallax effects.

A considerable number of short-duration microlensing events due to FFPs will be discovered by the Roman Space Telescope during its microlensing survey (see, e.g., Penny et al. 2019; Johnson et al. 2020). We note that Sumi et al. (2023) presented the first measurement of the mass function of FFPs and predicted that Roman could detect a significant number of these objects with masses down to that of Mars. Since measuring their parallax effects is crucial to correctly extract the mass and distance of the lens, possible joint observations of these events by Roman, LSST (LSST Science Collaboration et al. 2009), Euclid, and Chinese Space Station telescopes were proposed by Bachelet & Penny (2019), Ban (2020), Bachelet et al. (2022), and Yan & Zhu (2022). Also, Hamolli et al. (2013) simulated microlensing events due to FFPs by considering the parallax effect and discussed the best position of the Earth in its orbit around the Sun for measuring the parallax effect.

Simultaneous observations are not possible for some short-duration microlensing events: for instance, for those where either (i) their durations are very short, or (ii) their observing field is not observable by two telescopes simultaneously, or (iii) other telescopes have other priorities for their observations. Modeling such microlensing events leads to lensing parameters that deviate somewhat from their real values. We study this point (how far invisible parallax is destructive while interpreting short-duration events due to FFPs) in this work numerically, and we statistically evaluate the parallax-induced deviations of the inferred lensing parameters from observations.

In Section 2, we review the formalism for microlensing light curves by considering the parallax effect. In Section 3, we generate short-duration ($t_{\rm E} < 10$ days) microlensing events due to FFPs toward the Galactic bulge, and assume these events are observed only by the Roman telescope during one observing season of 62 days. We extract the parallax-affected events by evaluating $\Delta\chi^2$ values. To calculate the parallax-induced deviations in their lensing parameters, we fit simple Paczyński microlensing models to their simulated synthetic data. The statistical results are explained in Section 4. In the last section, we explain the results and conclusions.

2. Formalism: Microlensing and Parallax

In a microlensing event due to a pointlike source star, the magnification factor depends only on the lens–source relative distance projected on the plane of the sky and normalized to the Einstein radius, u, as given by

$$A(u) = \frac{u^2 + 2}{u\sqrt{u^2 + 4}}. \tag{1}$$

We first assume the observer is at the Sun's center (the so-called heliocentric frame). The heliocentric coordinate system is specified by three normal axes, i.e., ($\hat{n}_1$, $\hat{n}_2$, $\hat{z}$), where $\hat{z}$ is in the direction of the line of sight toward the source star. ($\hat{n}_1$, $\hat{n}_2$) describe the plane of the sky, where $\hat{n}_1$ is in the direction of increasing Galactic longitude and $\hat{n}_2$ is toward the Galactic north pole. In this system, the components of the lens–source relative trajectory projected on the plane of the sky, $\boldsymbol{u}_{\odot}$, are given by

$$\begin{aligned} u_{\odot,\hat{n}_1} &= \frac{t - t_0}{t_{\rm E}}\cos\xi - u_0 \sin\xi, \\ u_{\odot,\hat{n}_2} &= \frac{t - t_0}{t_{\rm E}}\sin\xi + u_0 \cos\xi, \end{aligned} \tag{2}$$

where $u_{\odot} = (u_0^2 + (t - t_0)^2/t_{\rm E}^2)^{1/2}$, t_0 is the time of closest approach, u_0 is the lens impact parameter, and ξ is the angle of projection of the lens–source relative trajectory on the $\hat{n}_1$ axis. $t_{\rm E}$ is the time taken to cross the angular Einstein radius at the lens–source relative velocity:

$$t_{\rm E} = \frac{\theta_{\rm E}}{\mu_{\rm rel,\odot}}, \qquad \theta_{\rm E} = \frac{R_{\rm E}}{D_{\rm l}} = \sqrt{\frac{4GM_{\rm l}}{c^2}\frac{D_{\rm ls}}{D_{\rm l}D_{\rm s}}}, \tag{3}$$

where G is the gravitational constant, c is the speed of light, $D_{\rm l}$ and $D_{\rm s}$ are the lens and source distances from the observer, and $D_{\rm ls} = D_{\rm s} - D_{\rm l}$. $\mu_{\rm rel,\odot}$ is the size of the lens–source angular velocity vector as measured in the heliocentric reference frame, and is given by

$$\boldsymbol{\mu}_{\rm rel,\odot} = \frac{\boldsymbol{v}_{\rm s,\,p} - \boldsymbol{v}_{\odot,p}}{D_{\rm s}} - \frac{\boldsymbol{v}_{\rm l,\,p} - \boldsymbol{v}_{\odot,p}}{D_{\rm l}}, \tag{4}$$

where $\boldsymbol{v}_{\rm l,p}$, $\boldsymbol{v}_{\rm s,p}$, and $\boldsymbol{v}_{\odot,p}$ are the velocity vectors of the lens, source, and Sun projected on the plane of the sky. Since the motion of the Sun around the Galactic center during a lensing event is linear, the lens trajectory with respect to the source star (as measured in the heliocentric coordinate frame) is a straight line with a constant relative velocity $\boldsymbol{\mu}_{\rm rel,\odot}$.

Now, we assume the observer is orbiting the Sun. The annual motion of the observer around the Sun changes $\boldsymbol{\mu}_{\rm rel,\odot}$ by

$$\boldsymbol{\mu}_{\rm rel,o} = \boldsymbol{\mu}_{\rm rel,\odot} + \frac{\pi_{\rm rel}}{1\ {\rm au}}\boldsymbol{v}_{{\rm o},p}, \tag{5}$$

where $\boldsymbol{v}_{{\rm o},p}$ is the observer's velocity with respect to the Sun projected on the plane of the sky, and $\pi_{\rm rel} = 1\ {\rm au}/D_{\rm l} - 1\ {\rm au}/D_{\rm s}$ is the relative parallax amplitude. Accordingly, the observer's motion around the Sun changes two components of $\boldsymbol{u}_{\rm o}$:

$$\begin{aligned} u_{{\rm o},\hat{n}_1} &= u_{\odot,\hat{n}_1} + \pi_{\rm E}\int_{t_0}^{t}\frac{v_{{\rm o},\hat{n}_1}}{1\ {\rm au}}dt, \\ u_{{\rm o},\hat{n}_2} &= u_{\odot,\hat{n}_2} + \pi_{\rm E}\int_{t_0}^{t}\frac{v_{{\rm o},\hat{n}_2}}{1\ {\rm au}}dt. \end{aligned} \tag{6}$$

These parallax-induced deviations vary periodically (the same as a sine function) with known amplitude $\pi_{\rm E} = \pi_{\rm rel}/\theta_{\rm E} = \sqrt{\pi_{\rm rel}/\kappa M_{\rm l}}$, where κ is a constant.

2.1. Case Study: Short-duration Microlensing Due to FFPs

Here, we aim to evaluate the second terms in Equation (6) (the parallax-induced deviations) in short-duration microlensing events due to FFPs. To project the observer's velocity vector on the sky, we first specify its components in the Galactic coordinate system. The Galactic coordinate system is described with three orthogonal directions (U, V, W), which are radial toward the Galactic center, clockwise tangential in the Galactic plane, and normal to the Galactic plane and toward the

Galactic north pole, respectively. The components of the observer's velocity in this coordinate system are given by

$$v_{o,U} = +V_o \sin\Omega \cos\theta_\oplus,$$
$$v_{o,V} = -V_o \cos\Omega,$$
$$v_{o,W} = -V_o \sin\Omega \sin\theta_\oplus, \quad (7)$$

where $\theta_\oplus = \pi/3$ is the angle between the plane of the Earth's orbit around the Sun and the Galactic plane, $V_o = R_o\,\omega$, $\Omega = \omega\,(t - t_0) + \phi_0$, $\omega = 2\pi/P_\oplus$ is Earth's angular velocity around the Sun, and $P_\oplus = 365.25$ days. ϕ_0 is an initial phase that describes Earth's velocity vector at the time of closest approach in the lensing formalism. R_o is the orbital radius of the observer around the Sun, which is the astronomical unit (1 au) when the observer is on the Earth and 1.01 au for the Roman telescope (from the L2 Lagrangian point). Here, we assumed that the observer is orbiting the Sun in the Earth's orbital plane and in a circular orbit.

According to the formalism introduced in the Appendix of Sajadian & Sahu (2023), we derive the components of the Earth's velocity projected on the plane of the sky (in the directions $\hat{n}_1$, $\hat{n}_2$) as

$$v_{o,\hat{n}_1} = \sin\alpha\; v_{o,U} - \cos\alpha\; v_{o,V},$$
$$v_{o,\hat{n}_2} = \sin b[\cos\alpha\; v_{o,U} + \sin\alpha\; v_{o,V}] + \cos b\;\; v_{o,W}. \quad (8)$$

Here, b is the apparent Galactic latitude of the line of sight of the source star, $\alpha \simeq \pi - l$, and l is the apparent Galactic longitude of this line of sight. Toward the Galactic bulge, $l \simeq 0$, $b \simeq 0$, and so $\alpha \simeq \pi$. Additionally, for short-duration microlensing events due to FFPs, $|t - t_0| \ll P_\oplus$. Considering these features and using Equation (8), the two parallax-induced deviations (given in Equation (6)) are

$$\delta u_{\hat{n}_1} \simeq -R'_o \pi_E(\sin\Omega - \sin\phi_0)$$
$$\simeq -R'_o \pi_E\Big[\omega(t - t_0)\cos\phi_0 - \tfrac{1}{2}\sin\phi_0\,\omega^2(t - t_0)^2\Big],$$
$$\delta u_{\hat{n}_2} \simeq \tfrac{\sqrt{3}}{2} R'_o \pi_E(\cos\Omega - \cos\phi_0)$$
$$\simeq \tfrac{\sqrt{3}}{2} R'_o \pi_E[-\omega(t - t_0)\sin\phi_0$$
$$- \tfrac{1}{2}\omega^2(t - t_0)^2\cos\phi_0\Big], \quad (9)$$

where $R'_o = R_o/1$ au and $\boldsymbol{u}_o = \boldsymbol{u}_\odot + \boldsymbol{\delta u}$. In these relations, although $\omega(t - t_0) \sim t_E/P_\oplus$ is very small, in short-duration microlensing events due to FFPs the parallax amplitudes ($\pi_E \propto 1/\sqrt{M_l}$) are considerable and larger than those in common microlensing events by 5 up to 3000 times for $M_l \in [0.01\,M_\oplus, 15\,M_J]$.

Hence, the parallax effect in microlensing events due to FFPs is not discernible, because two parallax-induced deviation terms (Equation (9))—as long as $t_E \ll P_\oplus$—behave linearly versus time without any bending or acceleration (by considering only first-order terms). In that case, $\boldsymbol{u}_o$ will be a straight line and the offered light curve will be symmetric about its peak. However, if $\pi_E \times t_E$ has the same order of magnitude as $P_\oplus$, i.e., $\pi_E \times t_E (= \pi_{rel}/\mu_{rel,o}) \sim P_\oplus$, then $\boldsymbol{\delta u}$ alters $\boldsymbol{u}_\odot$ considerably, which means $A(u_o)$ and $A(u_\odot)$ are different, although both of them are simple and symmetric. In such events the parallax effect is indistinguishable and invisible, but it changes the observed light curve and its parameters considerably. Accordingly, in short-duration events due to FFPs, $\delta u \propto \pi_{rel}$, which means parallax can cause large deviations when FFPs are close to the observer with high π_{rel} values. We examine these points in the next section based on a Monte Carlo simulation.

3. Monte Carlo Simulation: Microlensing due to FFPs by Roman

In this section we perform a Monte Carlo simulation from microlensing events due to FFPs that can be detected during the Roman microlensing survey. We assume that the Roman telescope takes data from these events during one observing season of 62 days along seven lines of sight toward the Galactic bulge and there are no follow-up observations of these events.

The details of these simulations can be found in our previous papers (see, e.g., Sajadian 2021a; Sajadian & Sangtarash 2023; Sajadian et al. 2023), so we briefly explain them here. To generate a microlensing event, we should choose (i) a source star along a given line of sight, and (ii) a lens object, and then (iii) determine the lensing parameters. We specify the distances of source stars (D_s) based on the overall mass density versus the distance from the observer along a given line of sight. Then, we determine the photometric properties of each source stars using the Besançon model, and accordingly the Galactic structure to which the source star belongs (Robin et al. 2003, 2012). In the next step, we indicate the distance of the lens from the observer (D_l) using the microlensing event rate function. We limit the masses of lenses to the range $M_l \in [0.01\,M_\oplus, 15\,M_J]$ and select them using a log-uniform mass function $dN/dM_l \propto M_l^{-1}$, in the same way as Johnson et al. (2020) and Sajadian (2021b). We determine the velocity components of the lens and source dispersion using the normal distributions whose widths are given by Robin et al. (2003). In short-duration microlensing events due to FFPs, the finite-source effect (Witt & Mao 1994) is considerable, since the angular source radius $\theta_\star$ normalized to the angular Einstein radius is $\rho_\star = \theta_\star/\theta_E \propto M_l^{-1/2}$. Therefore, we determine the microlensing magnification factor by considering finite-source size and using RTModel (Bozza 2010; Bozza et al. 2018). For these events we consider the parallax effect based on the formalism explained in the previous section. Since we aim to focus on events affected by the parallax, whereas this effect is unrecognizable while modeling (or when this effect should be ignored while inferring the lensing parameters), we exclude events that have $t_E > 10$ days. However, in the simulation 99% of simulated events due to FFPs with a log-uniform mass function had t_E less than 10 days.

In the next step, for each light curve we produce synthetic data points taken by the Roman telescope. We consider an observing season of duration $T_{obs} = 62$ days, and uniformly choose values of t_0 from the range $[0, T_{obs}]$. For each data point we determine the error bar in the magnification factor using $\sigma_A = A|1 - 10^{-0.4\,\sigma_m}|$, where A is the magnification factor. σ_m is the Roman photometric error, which is a function of the apparent magnitude in the Roman filter (W149; Figure 4 in Penny et al. 2019). The cadence between data points is fixed to 15.16 minutes.

In the simulation we determine the number of blending stars by integrating over the Galactic number density along a given line of sight to determine the projected surface one (Equations (2) and (3) in Sajadian & Poleski 2019). This surface density indicates the number of blending stars whose lights enter the

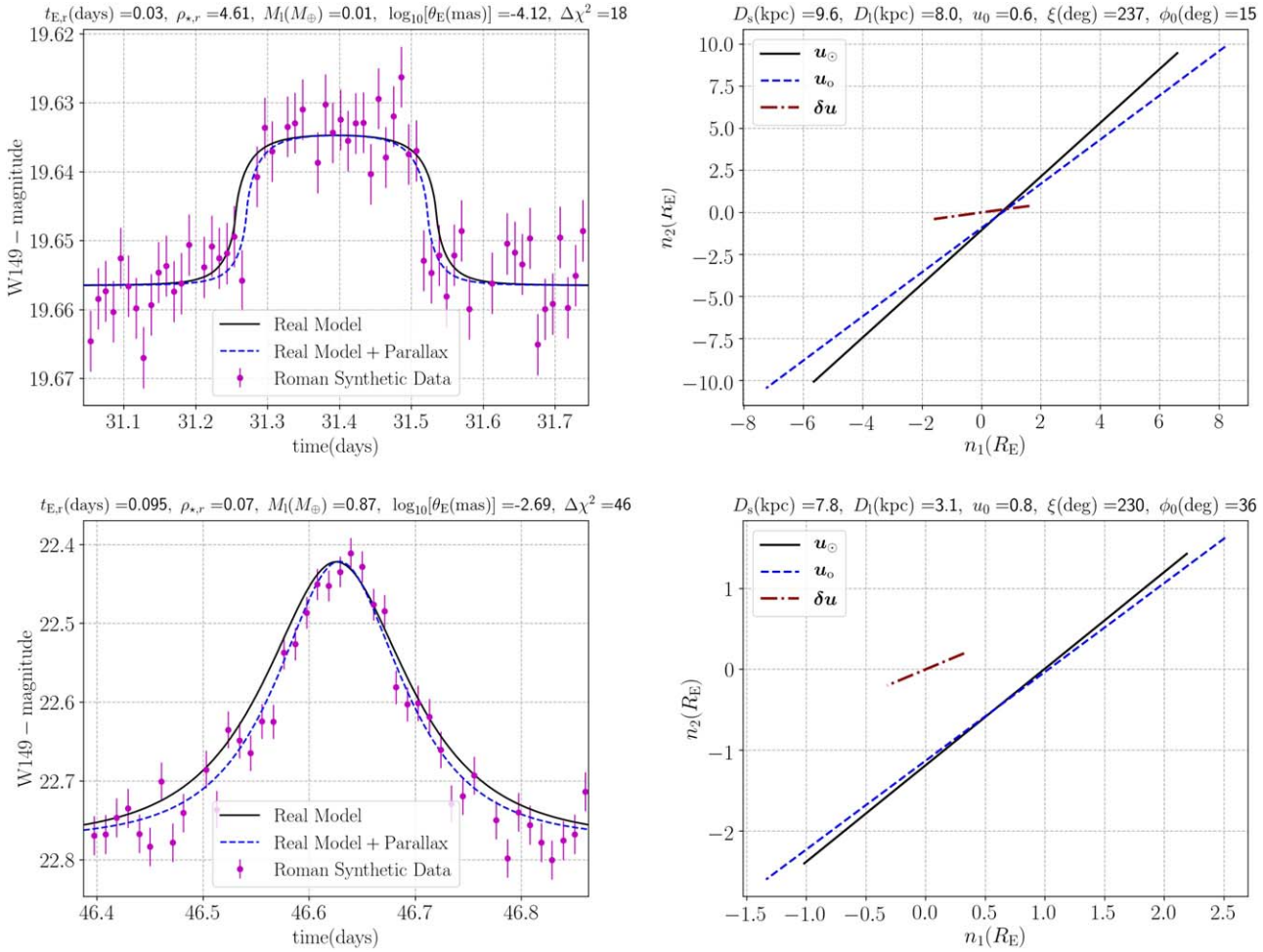

Figure 1. Left panels: two examples of microlensing light curves due to FFPs in which the parallax effects are not discernible. Right panels: their lens–source relative trajectories projected on the plane of the sky without (black solid lines, $\boldsymbol{u}_\odot$) and with (blue dashed lines, $\boldsymbol{u}_o$) considering the parallax effect. In these panels, the dark red dotted–dashed lines are $\boldsymbol{\delta u}$. The index r for parameters refers to their values in the real models.

point-spread function (PSF) of the source. The blending in the lensing formalism is usually evaluated by the factor f_{bl}, which is the ratio of the source flux (itself) to the total baseline flux that enters the source PSF. The higher the f_{bl} value, the smaller the number of blending stars. We perform this Monte Carlo simulation, and generate 9646 microlensing events due to FFPs with $t_E < 10$ days that are potentially discernible by the Roman telescope. The detectability criteria were explained in Sajadian (2021b).

For some of these events, the parallax effect does not change the shape of the light curve, and so ignoring the parallax effect for these events does not alter the inferred lensing parameters significantly. To extract these events we consider a criterion, i.e., the difference between χ^2_{real} and $\chi^2_{without}$ values from fitting the real model with parallax and without parallax (respectively) should be less than 100, i.e., $\Delta\chi^2 = |\chi^2_{real} - \chi^2_{without}| < 100$. Most of these events have either very short timescales (with sparse data points), or large finite-source sizes or faint source stars with high photometric error bars, which all result small $\Delta\chi^2$ values. Additionally, when $D_l \simeq D_s$, which produces very small π_{rel} values, the parallax amplitude decreases, and this effect will not change the microlensing light curve.

Two examples of these events can be found in Figure 1. In this figure, for two light curves (shown in the left panels), their lens–source relative trajectories with (blue dashed line, $\boldsymbol{u}_o$) and without (black solid line, $\boldsymbol{u}_\odot$) parallax effects are presented in the right panels. The parallax-induced deviations in the lens–source relative trajectories $\boldsymbol{\delta u}$ are depicted with dark red dotted–dashed lines. The lensing parameters used for these light curves are mentioned at the top of the plots. In these light curves high photometric errors and a small number of data points cause the parallax-induced deviations to be undetectable.

46.3% of all simulated events have $\Delta\chi^2 > 100$ and $t_E < 10$ days. For these events the parallax effect is invisible, but it changes their observed light curves considerably.

In Figure 2, we show the normalized distributions of some parameters from simulated microlensing events due to FFPs with light purple color. To study what kinds of simulated events are more affected with the parallax effect, in these plots the distributions of events with $\Delta\chi^2 > 100$ (and $\Delta\chi^2 < 100$) are plotted with green (and black) histograms. To better compare these distributions, in Table 1 we report the average values of the parameters whose distributions are plotted in Figure 2. In this table three rows (from top to bottom) contain the average values due to all simulated events (with light purple histograms), parallax-affected events (green histograms) and unaffected ones (black ones).

Accordingly, most of the events in which $D_l \lesssim 3$ kpc (or $\pi_{rel} \gtrsim 0.2$ mas) and $t_E \gtrsim 3$ days (which have a greater number of data points) are affected by parallax with $\Delta\chi^2 > 100$. Also, the

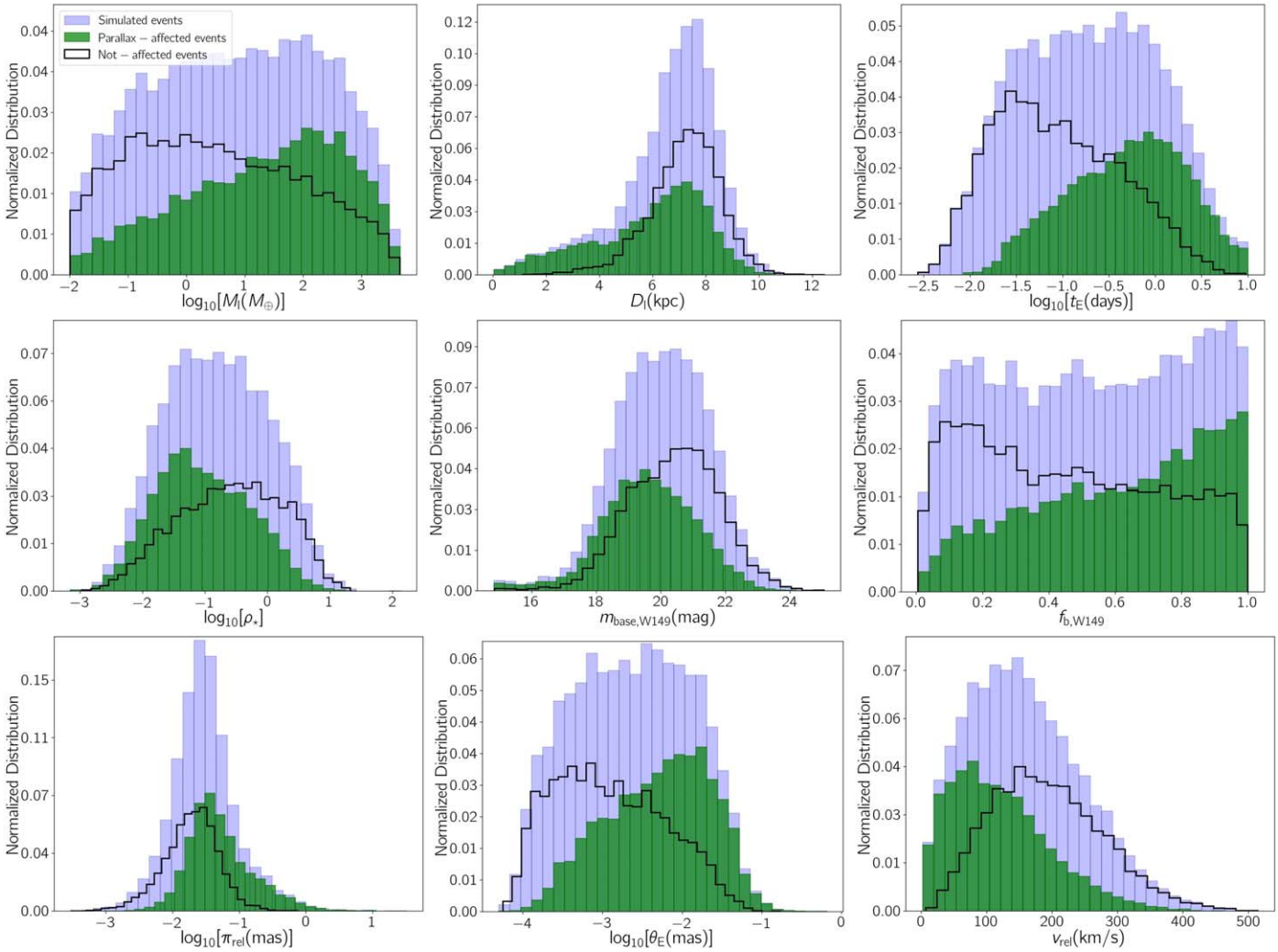

Figure 2. The light purple histograms are the normalized distributions of some parameters due to all simulated microlensing events, which are described in Section 3. The normalized distributions of the events whose light curves are (and are not) affected by parallax effects are shown with green (and black) histograms. Green histograms are with $\Delta\chi^2 > 100$ and black ones with $\Delta\chi^2 < 100$ as the criteria.

Table 1
Average Values of the Parameters Whose Distributions are Shown in Figure 2

Parameters/from Events	$\log_{10}[\overline{M_l}]$ ($M_\oplus$)	$\overline{D_l}$ (kpc)	$\log_{10}[\overline{t_E}]$ (days)	$\log_{10}[\overline{\rho_\star}]$	$\overline{m_{base}}$ (mag)	$\overline{f_{bl}}$	$\log_{10}[\overline{\pi_{rel}}]$ (mas)	$\log_{10}[\overline{\theta_E}]$ (mas)	$\overline{v_{rel}}$ (km s^{-1})
All events	2.33	6.58	−0.16	−0.14	20.02	0.53	−1.12	−2.09	159.10
Parallax-affected events	2.46	5.86	0.07	−0.40	19.60	0.61	−0.88	−1.90	120.91
Unaffected events	2.16	7.19	−0.55	0.01	20.38	0.45	−1.55	−2.39	192.05

events due to faint or highly blended source stars, or those with $\rho_\star \gtrsim 3$ are less affected by parallax (e.g., the top event in Figure 1). In fact, when the normalized source radius is large, the magnification factor is low because it is estimated as $1 + 2/\rho_\star^2$ (Gould & Gaucherel 1996; Agol 2003), so variations in the lens–source relative trajectory do not change the light curve much.

In the next section, we focus on the microlensing events with $\Delta\chi^2 > 100$ and study the parallax-induced deviations in their lensing parameters by finding the best-fitted simple Paczyński light curves for these events.

3.1. Fitting Simple Paczyński Microlensing Models

For each of the simulated microlensing events due to FFPs with $t_E < 10$ days and $\Delta\chi^2 > 100$, we find the best-fitted simple Paczyński microlensing models using the Python-based package `emcee`[1] (Foreman-Mackey et al. 2013). For fitting a simple microlensing model there are five parameters: t_E, $\rho_\star$, t_0, u_0, and f_b. We exclude the apparent baseline magnitude due to all blending stars in the W149 filter, m_{base}, because the parallax does not change this parameter. To find the best-fitted microlensing models with five free parameters, 40 chains (i.e., Nwalkers = 40 in the `emcee` code) of 10,000 steps each were sufficient. We ignore the limb-darkening effect for source stars, and simulate synthetic data points for light curves with $\rho_\star < 1$ in the time interval $[-2.5t_E + t_0, 2.5t_E + t_0]$, and the others in the time interval $[-2.5t_\star + t_0, 2.5t_\star + t_0]$, where $t_\star = t_E \times \rho_\star$.

[1] https://emcee.readthedocs.io/en/stable/

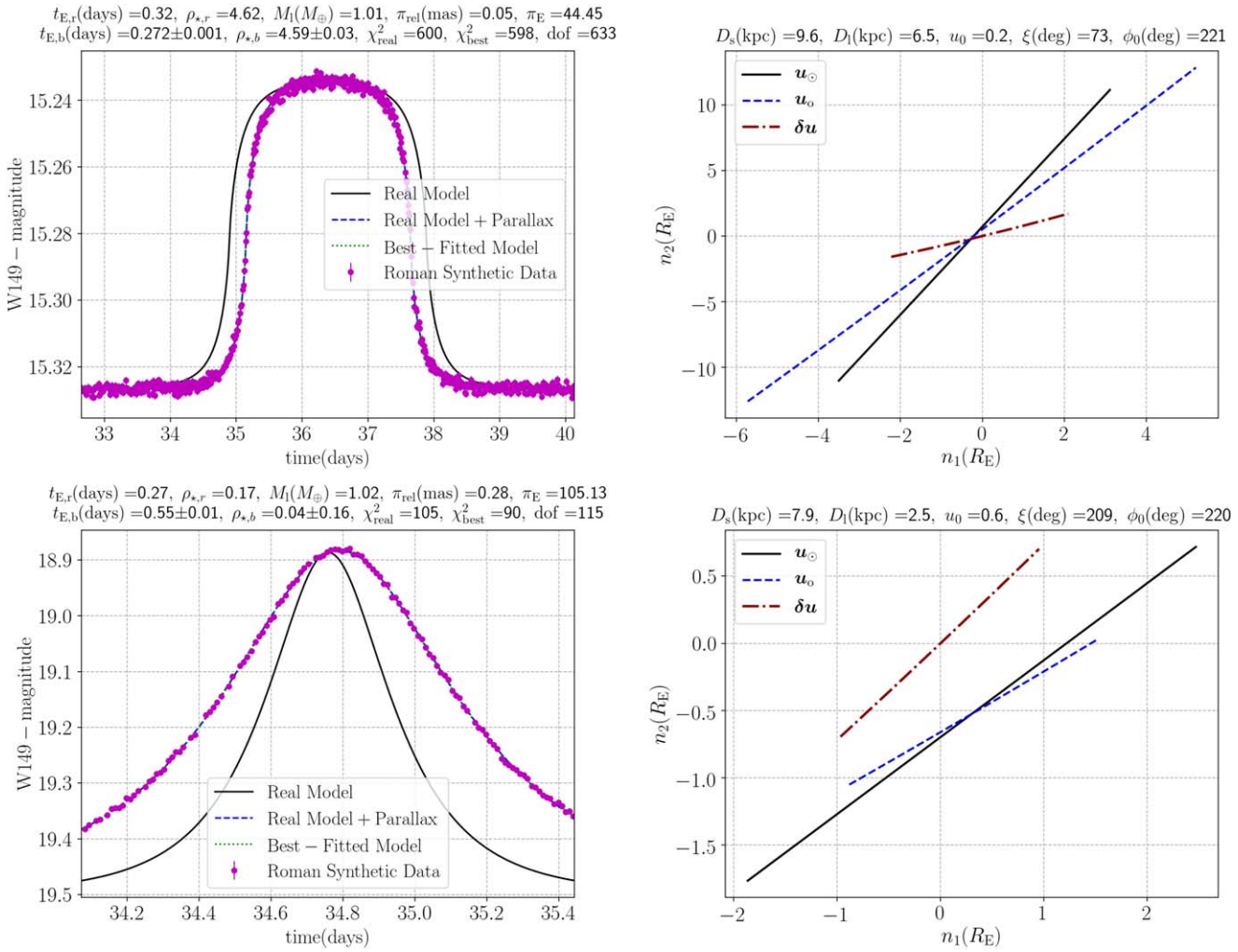

Figure 3. Similar to Figure 1. In these two short-duration microlensing light curves the parallax changes their widths significantly. The index b for t_E and $\rho_\star$ refers to their values in the best-fitted simple microlensing models. The best-fitted light curves are depicted by green dotted curves. In the titles "dof" refers to the degrees of freedom.

The two parameters t_E and $\rho_\star$ are functions of the lens mass and its distance. Hence, the parallax-induced deviations from these two parameters directly lead to misinterpretation of the lens object. From simulations, we found that in events where $\boldsymbol{u}_\odot$ and $\boldsymbol{\delta u}$ are parallel, i.e., $|\xi - \phi_0| \simeq 0$ or 180°, the widths of observed light curves change significantly and lead to the highest deviations in either t_E or $\rho_\star$. Two examples of such events are presented in Figure 3. Here the best-fitted light curves are shown as green dotted curves. $t_{E,b}$ and $\rho_{\star,b}$ are the Einstein crossing time and the normalized source radius due to the best-fitted models, which are mentioned in the second lines of the left panels' titles. To evaluate the goodness of the fitted models, we report the χ^2_{real} and χ^2_{best} values due to the real and best-fitted models (blue dashed and green dotted curves respectively), and the number of degrees of freedom (dof) in the titles.

As mentioned in the previous section, when π_{rel} is large (the lens object is close to the observer) the parallax-induced deviations in the microlensing light curves are relatively large so that most of lensing parameters due to the best-fitted models are different from the real ones. Two examples of such events are presented in Figure 4. The statistical results from this Monte Carlo simulation are reported in the next section.

4. Statistical Results

After indicating the best-fitted simple models for the simulated events with $\Delta\chi^2 > 100$, we statistically investigate the fractions of events in which the best-fitted lensing parameters are considerably different from the real ones. These fractions are reported in Table 2. In this regard, we define the relative variations in the lensing parameters, e.g., $\delta t_E = |t_{E,r} - t_{E,b}|/t_{E,r}$. Here, $t_{E,r}$ and $t_{E,b}$ are the Einstein crossing times from the real lensing model with parallax and the best-fitted simple model, respectively. Hence, the indices r and b (throughout the paper) refer to the real and best-fitted models. In the same way, we define the relative deviations in other lensing parameters as $\delta\rho_\star = |\rho_{\star,r} - \rho_{\star,b}|/\rho_{\star,r}$, $\delta u_0 = |u_{0,r} - u_{0,b}|/u_{0,r}$, $\delta t_0 = |t_{0,r} - t_{0,b}|/t_{0,r}$, and $\delta f_{bl} = |f_{bl,r} - f_{bl,b}|/f_{bl,r}$.

According to Table 2, the fraction of events in which the times of closest approach are shifted by $\delta t_0 \gtrsim 0.3$ is only 0.2%. The most affected parameter (by parallax) is $\rho_\star$. In 56.9% of events with $\Delta\chi^2 > 100$ the relative deviation $\delta\rho_\star$ is larger than 0.3. 8.0% of the parallax-affected events have $\delta t_E > 0.3$.

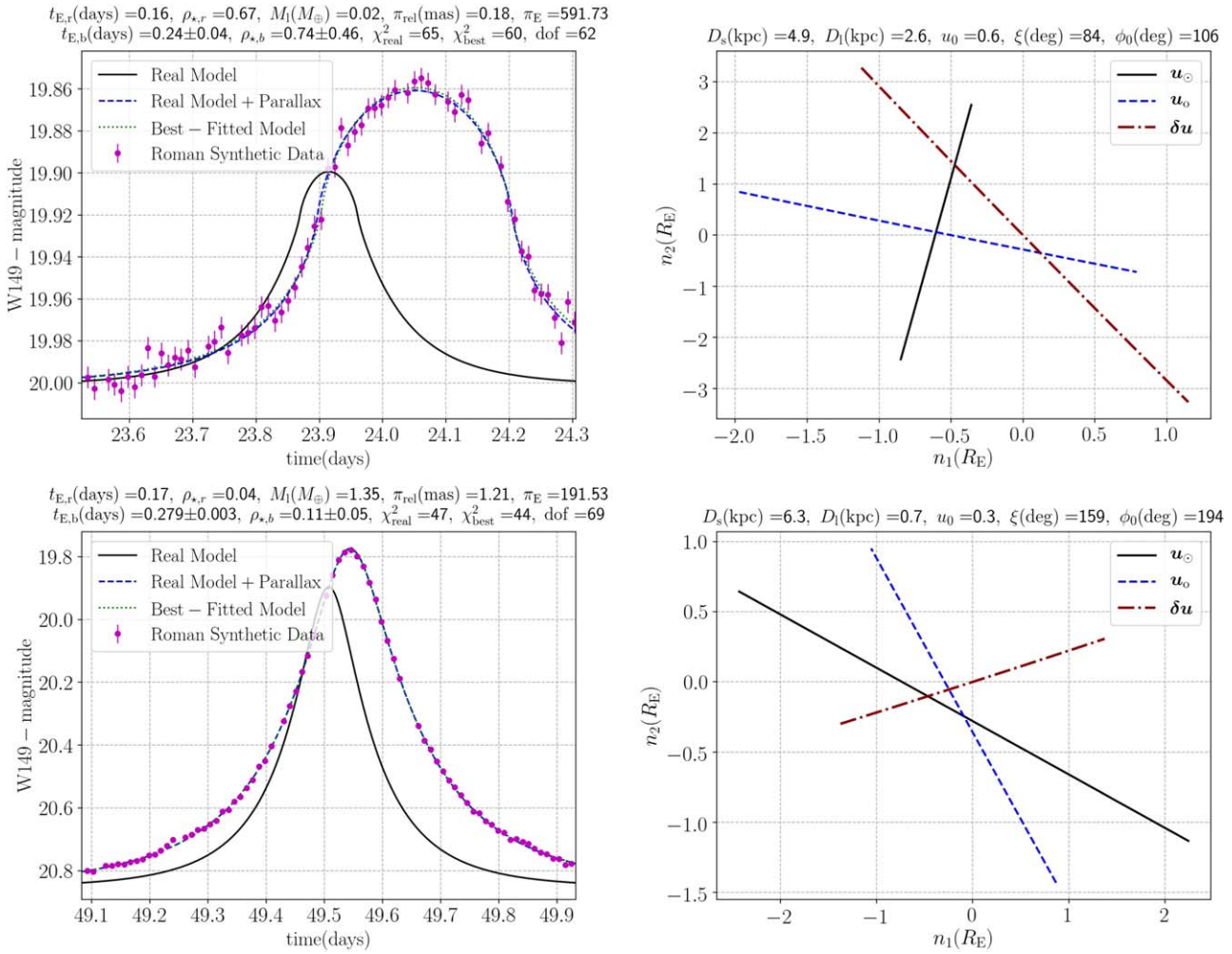

Figure 4. Similar to Figure 3. In these two microlensing events the parallax-induced deviations are significant, because in these events the lens object is close to the observer, which produces large π_{rel} values.

Table 2
Statistical Results from the Monte Carlo Simulation

	δt_E	$\delta\rho_\star$	δu_0	δt_0	δf_{bl}	δt_E and $\delta\rho_\star$
>0.02	73.7	83.6	63.2	3.6	52.1	62.6
>0.05	46.7	75.6	43.3	1.5	31.8	36.8
>0.1	26.8	68.8	29.4	0.7	18.6	19.8
>0.3	8.0	56.9	14.7	0.2	4.8	4.9
>0.5	3.8	48.7	10.1	0.1	1.9	1.9
>0.7	1.9	41.3	7.5	0.1	0.8	0.8

Note. Each entry is the fraction of simulated events with $\Delta\chi^2 > 100$ in which the given relative deviations (its column) are larger than the given threshold (its row).

Deviations in t_E and $\rho_\star$ lead to misinterpreting the lens object (its mass and distance). According to the simulation, we found that in 4.9% of simulated parallax-affected events with $\Delta\chi^2 > 100$, both relative deviations δt_E and $\delta\rho_\star$ were greater than 0.3.

The fraction of parallax-affected events as a function of four relevant parameters is plotted in Figure 5. In each panel, the three lines correspond to three different criteria to extract the affected events, which are: (i) gray solid lines show the fractions of events with $\Delta\chi^2 > 100$, (ii) red dashed lines represent the fraction of events with $\Delta\chi^2 > 100$ and $\delta t_E > 0.02$, and (iii) green dotted–dashed lines reveal the fraction of events with $\Delta\chi^2 > 100$ and $\delta\rho_\star > 0.02$. Four points from different panels of this figure are mentioned below.

1. According to the top left panel: the events with higher π_{rel} values (due to closer lens objects) are more affected by the parallax effect. According to the discussion in the previous sections, in short-duration microlensing events due to FFPs the parallax-induced deviation $\boldsymbol{\delta u}$ is almost a straight line, and $\delta u \propto \pi_{rel}$. By increasing π_{rel}, the relative deviations in both t_E and $\rho_\star$ grow. We also represent the scatter plot of δt_E versus D_l in the top panel of Figure 6, which emphasizes this point as well.
2. More massive lens objects produce longer microlensing events with smaller finite-source size and lower π_E. Hence, the lens mass has three effects on parallax-induced deviations. (i) Generally, longer events have higher numbers of data points and $\Delta\chi^2$ values. (ii) For longer microlensing events the approximations in Equation (9) are not valid, and by considering more terms in these expansions, δu will reduce by increasing the lens mass. (iii) The events with lower $\rho_\star$ values have on average higher magnification factors and are more sensitive to variations in parameters, especially $\rho_\star$. Considering all of these points, longer events due to

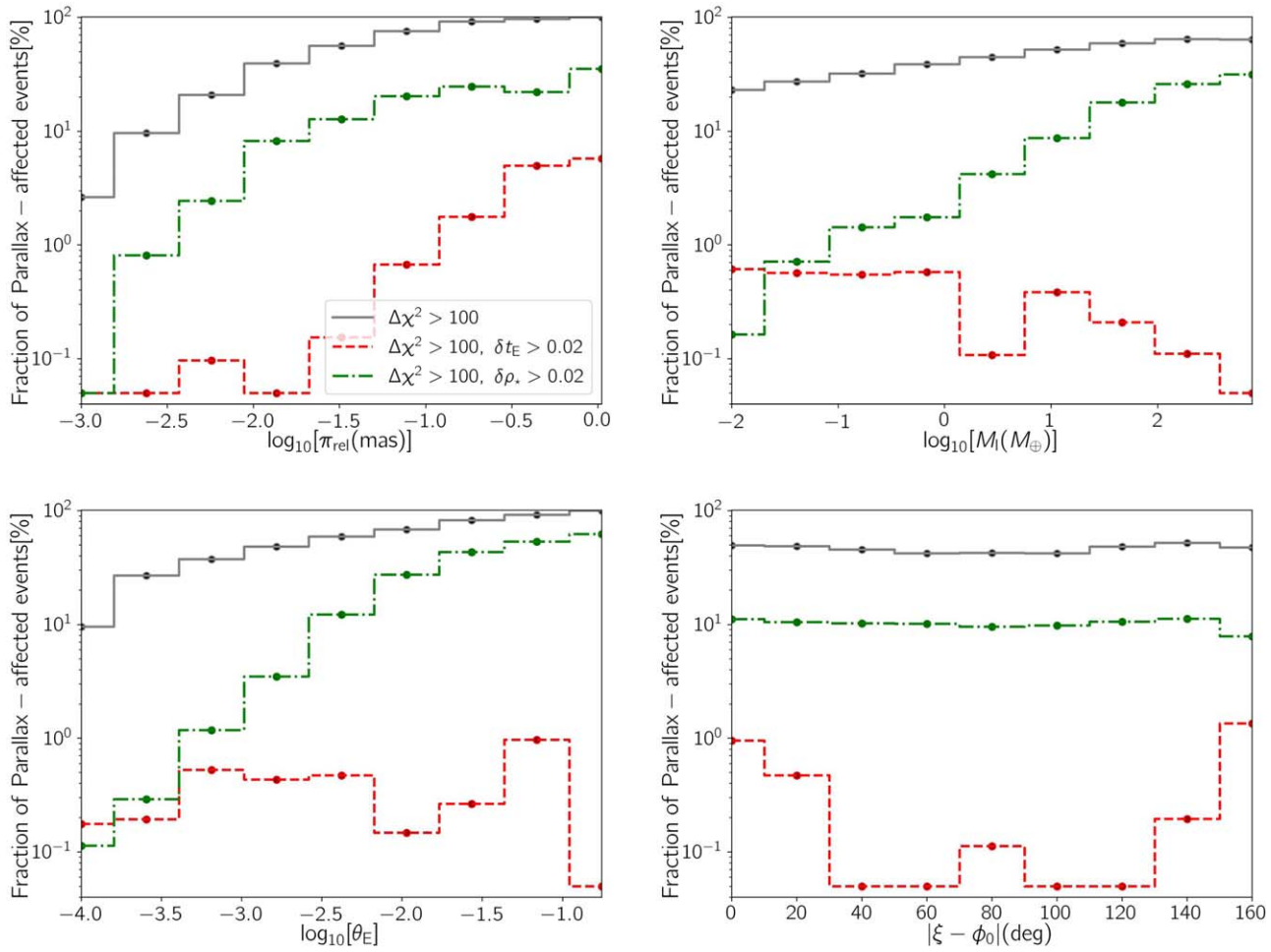

Figure 5. The fraction of simulated events due to FFPs that are affected by parallax as a percentage. Here, we have three definitions to extract the parallax-affected events: (i) $\Delta\chi^2 > 100$ (gray solid lines), (ii) $\Delta\chi^2 > 100$ and $\delta t_{\rm E} > 0.02$ (red dashed lines), and (iii) $\Delta\chi^2 > 100$ and $\delta\rho_\star > 0.02$ (green dotted–dashed lines).

more massive lens objects have lower $\delta t_{\rm E}$ (see also the bottom panel of Figure 6), but higher $\delta\rho_\star$, as depicted in the top right panel of Figure 5.

3. According to the bottom left panel of Figure 5, the events with larger finite-source sizes (with smaller $\theta_{\rm E}$ values) are less affected by parallax. As discussed in the previous section, the magnification factor due to large $\rho_\star$ is low and depends approximately on the source size itself (Gould & Gaucherel 1996; Agol 2003), and different lens trajectories emanating from large source disks have similar light curves. On the other hand, the magnification factor for such events is not high (very close to one), which causes, on average, higher photometric errors and lower $\Delta\chi^2$ values. We note that, considering (i) $\theta_{\rm E} = \sqrt{\kappa\, M_{\rm l}\, \pi_{\rm rel}}$ and (ii) that the two factors of the lens mass and the relative parallax have inverse effects on $\delta t_{\rm E}$, $\delta t_{\rm E}$ is not very sensitive to $\theta_{\rm E}$.
4. The last panel of Figure 5 emphasizes that the relative deviation $\delta t_{\rm E}$ additionally depends on the angle between the lens–source relative trajectory and the parallax vector ($|\xi - \phi_0|$). When $\boldsymbol{u}_\odot$ and $\boldsymbol{\delta u}$ are parallel ($|\xi - \phi_0| \simeq 0$ or 180°) the width of light curves and especially $t_{\rm E}$ changes considerably.

There are some other correlations between the real parameters and the relative deviations in the lensing parameters. These correlations reveal in what kind of short-duration microlensing events the indiscernible parallax effect actually changes each of lensing parameters. In Figure 7 we show the correlation matrix between relative deviations in the lensing parameters in the logarithmic scale (i.e., $\log_{10}[\delta t_{\rm E}]$, $\log_{10}[\delta\rho_\star]$, $\log_{10}[\delta u_0]$, $\log_{10}[\delta t_0]$, and $\log_{10}[f_{\rm bl}]$) and the eight relevant and physical parameters of simulated events ($\log_{10}[M_{\rm l}]$, $D_{\rm l}$, $\log_{10}[t_{\rm E}]$, $m_{\rm base}$, $\log_{10}[\pi_{\rm E}]$, $\log_{10}[\pi_{\rm rel}]$, $\log_{10}[\theta_{\rm E}]$, and $\log_{10}[\rho_\star]$). The correlation coefficients that are mentioned in the color bar are in the range $[-1, +1]$. A positive (negative) correlation between two entries means that values of the first one are rising (falling) as those in the second one increase. A correlation coefficient of zero means there is no correlation between the given entries.

The highest correlation for the relative deviations for the Einstein crossing time is 0.5 and with $D_{\rm l}$, and as a result $\log_{10}[\pi_{\rm rel}]$ and $\log_{10}[\pi_{\rm E}]$, as emphasized in the previous section.

The relative deviation in the source radius is highly correlated with $\log_{10}[\theta_{\rm E}]$ and $\log_{10}[\rho_\star]$ with a correlation coefficient of ± 0.6. There are weaker and positive correlations between it and $\log_{10}[t_{\rm E}]$ and the lens mass.

The relative deviation in the lens impact parameter (δu_0) is correlated with $\log_{10}[\pi_{\rm E}]$ and $\log_{10}[M_{\rm l}]$ with correlation coefficients of ± 0.5.

With regard to the relative deviation in the time of closest approach, the highest correlation is 0.6 and with $\log_{10}[t_{\rm E}]$.

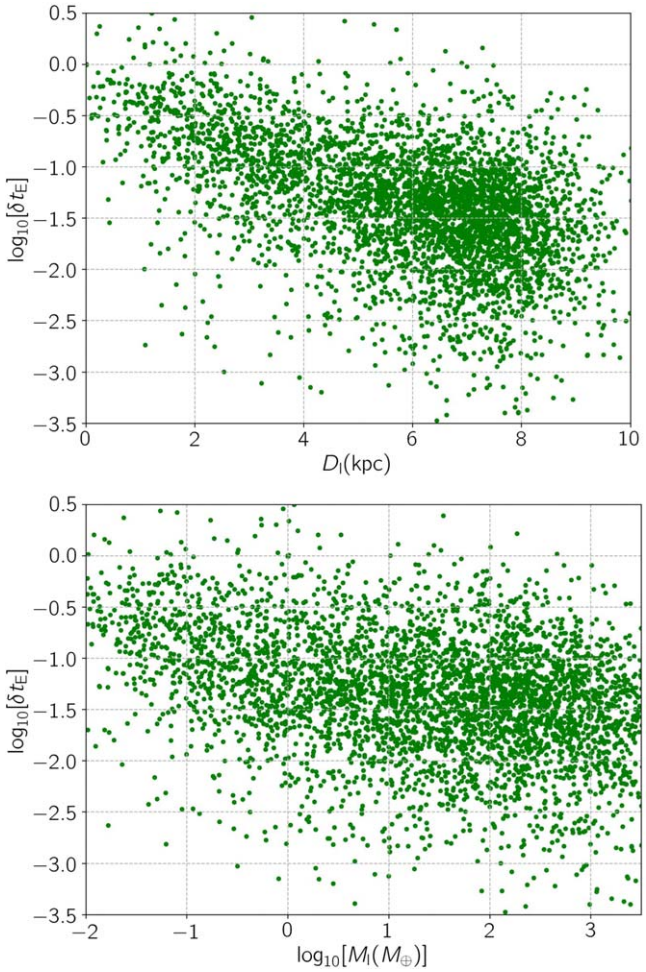

Figure 6. Scatter plot of the relative deviation in the Einstein crossing time $\delta t_{\rm E}$ vs. the two parameters $D_{\rm l}$ and $\log_{10}[M_{\rm l}(M_\oplus)]$.

Finally, the relative deviation in the blending factor is highly correlated with δu_0, which is 0.6. We note that the blending effect creates a degeneracy between parameters in microlensing events due to FFPs, especially those with considerable finite-source sizes (Mróz et al. 2020; Sajadian 2023), which creates these correlations between relative deviations. The microlensing events due to fainter source stars have higher relative deviations in $t_{\rm E}$, $\rho_\star$, t_0, and $f_{\rm b}$.

To estimate the number of FFPs that will be detected by the Roman telescope through its microlensing survey with parameters that are misinterpreted because of the indiscernible parallax effect, we use the predictions offered by Johnson et al. (2020). Accordingly, the Roman telescope will detect $N_{\rm FFP}=897$ FFPs in the mass range $[0.1M_\oplus, 1000M_\oplus]$ by assuming a log-uniform mass function for them (see Table 2 of Johnson et al. 2020). According to our simulation in the same mass range, $f_1=36.5\%$ of such events have $\Delta\chi^2>100$. In $f_2=13.9\%$, 3.1%, and 1.1% of these events, indistinguishable parallax effects make the relative deviations in both $t_{\rm E}$ and $\rho_\star$ larger than 0.1, 0.3, and 0.5 respectively. The number of parallax-affected FFPs detectable by the Roman telescope can be estimated as $N=N_{\rm FFP}\times f_1\times f_2$. Hence, 46, 10, and 4 of these FFPs that are discovered through the Roman microlensing survey will be affected by invisible parallax so that both $\delta t_{\rm E}$ and $\delta\rho_\star$ are larger than 0.1, 0.3, and 0.5, respectively.

5. Conclusions

Our Galaxy contains trillions of FFPs (Sumi et al. 2023). Gravitational microlensing is a powerful technique to discover such isolated and dark objects and even less-massive ones (see, e.g., Sumi et al. 2011; Mróz et al. 2017). Although the James Webb Space Telescope can find planetary-mass objects as small as 0.6 Jupiter masses that are very young and located in regions of active stellar formation (Pearson & McCaughrean 2023), gravitational microlensing is still the only way to find cold and dark small bodies in our Galaxy regardless of their ages and locations.

In the short-duration microlensing events due to FFPs with planetary masses (i.e., $M_{\rm l}\in[0.01\ M_\oplus,\ 15\ M_{\rm J}]$ where $M_{\rm J}$ is Jupiter's mass), the parallax amplitudes are higher than those in common events (due to M dwarfs with mass $\sim0.3\ M_\odot$) by [5, 3000] times. On the other hand, the duration of such events is very short as it is scaled by $t_{\rm E}\propto\sqrt{M_{\rm l}}$, and is mostly up to a few days. Considering the orbital period of the Earth around the Sun ($P_\oplus$), discerning the parallax effect in such short-duration events is barely possible.

At first glance, the parallax effect is not recognizable in such events and cannot help to resolve the microlensing degeneracy. But looking more closely, although the duration of these events is short and we cannot model and discern the annual parallax, this effect changes the shapes of observed light curves and their lensing parameters, because of large $\pi_{\rm E}$ values in these events.

In a short-duration microlensing events due to FFPs, if $t_{\rm E}\ll P_\oplus$ we can expand the parallax-induced deviation in the lens–source relative trajectory ($\boldsymbol{\delta u}$). By considering only the first-order term in $t_{\rm E}/P_\oplus$, this deviation makes a straight line without bending whose size is $\propto\pi_{\rm rel}$. Hence, the observer's motion around the Sun alters the lens–source relative trajectory in this event as $\boldsymbol{u}_{\rm o}=\boldsymbol{u}_\odot+\boldsymbol{\delta u}$, and as a result its light curve too. The point is that both light curves $A(u_{\rm o})$ and $A(u_\odot)$ are simple with different lensing parameters. If only one observer takes data from these short-duration events due to FFPs, the indiscernible parallax effect deviates the best-fitted lensing parameters from their real values.

In this work, we have evaluated the parallax-induced deviations in these events statistically. We simulated microlensing events due to FFPs that have $t_{\rm E}<10$ days and assumed that the Roman telescope would be the only observer of these events. We expect that some of short-duration microlensing events that will be alerted by Roman will not be followed up by other telescopes (in different orbits around the Sun), for instance events with very short timescales, or follow-up telescopes may have other priorities at the time of the Roman observations.

46.3% of these simulated events had $\Delta\chi^2=|\chi^2_{\rm real}-\chi^2_{\rm without}|>100$ (where $\chi^2_{\rm real}$ and $\chi^2_{\rm without}$ are the χ^2 values from fitting the real model with and without the parallax effect). These events mostly were due to FFPs close to the observer, $D_{\rm l}\lesssim3$ kpc (which had $\pi_{\rm rel}\gtrsim0.2$ mas). Also the events due to either faint or highly blended source stars, or those with $\rho_\star\gtrsim3$ are less affected by parallax (see Figure 2). We found that when the parallax vector and the lens–source trajectory were parallel, the widths of light curves changed significantly (see Figure 3).

For parallax-affected events with $\delta\chi^2>100$, we inferred the best-fitted simple Paczyński microlensing models and evaluated the relative deviations in the lensing parameters, i.e., $\delta t_{\rm E}$, $\delta\rho_\star$, δu_0, δt_0, and $\delta f_{\rm bl}$. We concluded that $\rho_\star$ is the most affected parameter so that $\delta\rho_\star>0.3$ in 56.9% of events. Also, the time

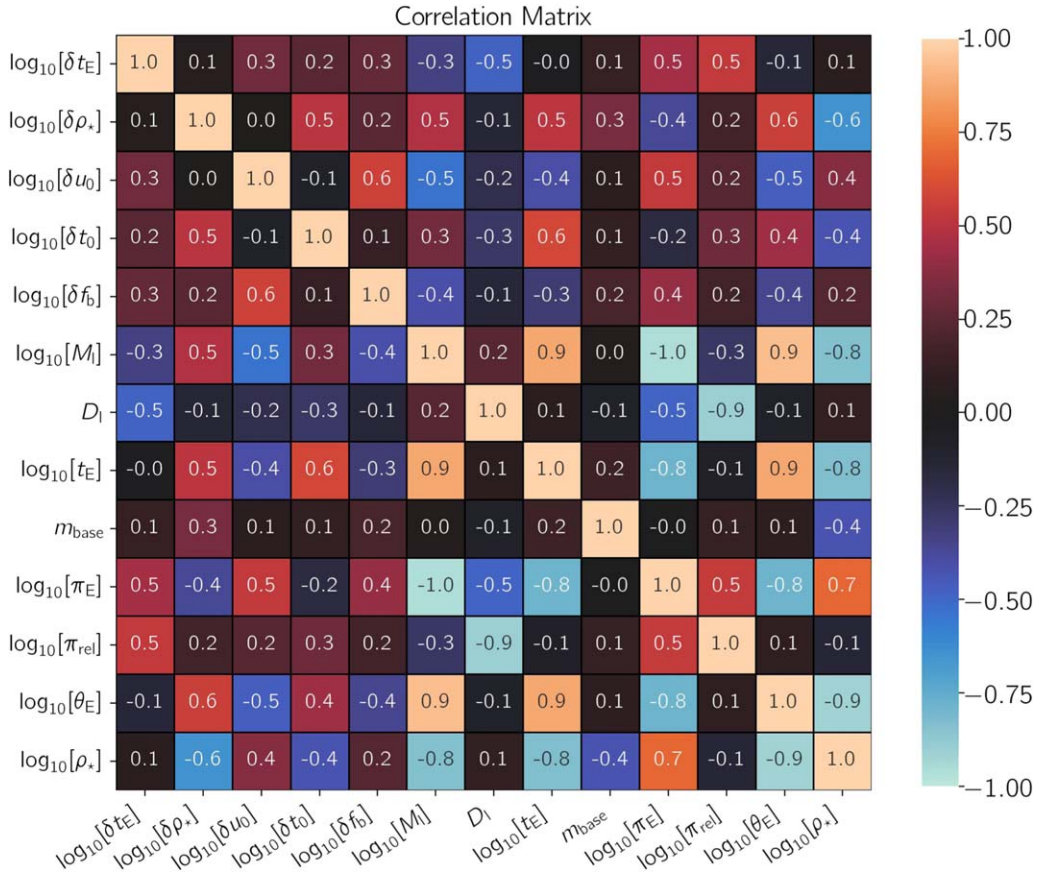

Figure 7. The correlation matrix between the relative deviations in the lensing parameters (the first five rows) due to the indiscernible parallax effects and the relevant and physical parameters of simulated events (the other rows).

of closest approach t_0 was the least affected parameter, so that $\delta t_0 > 0.3$ occurred only in 0.2% of events.

We estimated that 46 microlensing events due to FFPs that will be discovered by Roman will be affected by missing parallax, so that relative deviations in both t_E and $\rho_\star$ are larger than 0.1. This number of FFPs whose light curves (and lensing parameters) are affected by the parallax effect reveals the importance of making simultaneous and dense (with a short cadence) observations of microlensing events alerted by Roman to capture the parallax deviations in short-duration microlensing events due to FFPs. In this regard, the extra observations should be made by observers circling the Sun in different orbits from the Roman orbit.

All simulations that have been done for this paper are available at the GitHub and Zenodo addresses: https://github.com/SSajadian54/FFPs_parallax/ and https://zenodo.org/record/8342045 (Sajadian 2024).

ORCID iDs

Parisa Sangtarash https://orcid.org/0009-0007-4190-1269
Sedighe Sajadian https://orcid.org/0000-0002-2859-1071

References

Agol, E. 2003, ApJ, 594, 449
Alcock, C., Allsman, R. A., Alves, D., et al. 1995, ApJL, 454, L125
An, J. H., Albrow, M. D., Beaulieu, J. P., et al. 2002, ApJ, 572, 521
Bachelet, E., & Penny, M. 2019, ApJL, 880, L32
Bachelet, E., Specht, D., Penny, M., et al. 2022, A&A, 664, A136
Ban, M. 2020, MNRAS, 494, 3235
Bozza, V. 2010, MNRAS, 408, 2188
Bozza, V., Bachelet, E., Bartolić, F., et al. 2018, MNRAS, 479, 5157
Carroll, B. W., & Ostlie, D. A. 2006, An Introduction to Modern Astrophysics and Cosmology (Cambridge: Cambridge Univ. Press)
Dominik, M., Jorgensen, U. G., Horne, K., et al. 2008, arXiv:0808.0004
Einstein, A. 1936, Sci, 84, 506
Foreman-Mackey, D., Hogg, D. W., Lang, D., & Goodman, J. 2013, PASP, 125, 306
Gaia Collaboration, Vallenari, A., Brown, A. G. A., et al. 2023, A&A, 674, A1
Gaudi, B. S. 2012, ARA&A, 50, 411
Gould, A. 1992, ApJ, 392, 442
Gould, A. 1994, ApJL, 421, L75
Gould, A. 1995, ApJL, 441, L21
Gould, A. 1999, ApJ, 514, 869
Gould, A., & Gaucherel, C. 1996, arXiv:astro-ph/9606105
Hamolli, L., Hafizi, M., De Poalis, F., & Nucita, A. A. 2013, BlgAJ, 19, 34
Hirao, Y., Bennett, D. P., Ryu, Y.-H., et al. 2020, AJ, 160, 74
Johnson, S. A., Penny, M., Gaudi, B. S., et al. 2020, AJ, 160, 123
Koshimoto, N., Sumi, T., Bennett, D. P., et al. 2023, AJ, 166, 107
Liebes, S. 1964, PhRv, 133, B835
LSST Science Collaboration, Abell, P. A., Allison, J., et al. 2009, arXiv:0912.0201
Mróz, P., Poleski, R., Han, C., et al. 2020, AJ, 159, 262
Mróz, P., Udalski, A., Skowron, J., et al. 2017, Natur, 548, 183
Pearson, S. G., & McCaughrean, M. J. 2023, arXiv:2310.01231
Penny, M. T., Gaudi, B. S., Kerins, E., et al. 2019, ApJS, 241, 3
Perryman, M. A. C., Lindegren, L., Kovalevsky, J., et al. 1997, A&A, 323, L49
Refsdal, S. 1964, MNRAS, 128, 295
Refsdal, S. 1966, MNRAS, 134, 315
Robin, A. C., Marshall, D. J., Schultheis, M., & Reylé, C. 2012, A&A, 538, A106
Robin, A. C., Reylé, C., Derrière, S., & Picaud, S. 2003, A&A, 409, 523
Sajadian, S. 2021a, MNRAS, 508, 5991
Sajadian, S. 2021b, MNRAS, 506, 3 615
Sajadian, S. 2023, MNRAS, 521, 6383

Sajadian, S. 2024, FFP_Microlensing_Parallax, v1, Zenodo, doi:10.5281/zenodo.10827255
Sajadian, S., Mahmoudzadeh, A., & Moein, S. 2023, AJ, 166, 202
Sajadian, S., & Poleski, R. 2019, ApJ, 871, 205
Sajadian, S., & Sahu, K. C. 2023, AJ, 165, 96
Sajadian, S., & Sangtarash, P. 2023, MNRAS, 520, 5613
Shvartzvald, Y., Yee, J. C., Skowron, J., et al. 2019, AJ, 157, 106
Smith, M. C., Belokurov, V., Evans, N. W., Mao, S., & An, J. H. 2005, MNRAS, 361, 128
Sumi, T., Kamiya, K., Bennett, D. P., et al. 2011, Natur, 473, 349
Sumi, T., Koshimoto, N., Bennett, D. P., et al. 2023, AJ, 166, 108
Witt, H. J., & Mao, S. 1994, ApJ, 430, 505
Yan, S., & Zhu, W. 2022, RAA, 22, 025006
Zang, W., Shvartzvald, Y., Wang, T., et al. 2020, ApJ, 891, 3